The Tálar Caldera and its products: the southernmost centre of the Altiplano-Puna Volcanic Complex ignimbrite flare-up (Central Andes)

Jorge E. Romero[1]*, José A. Naranjo[2], Laurie Brown[3], Alexandre Corgne[4], Lewis Hughes[5], Carlos F. Ramírez[6].

[1]Instituto de Ciencias de la Ingeniería, Universidad de O'Higgins. Libertador Bernardo O'Higgins 611, Rancagua, Chile. jorge.romero@uoh.cl

[2]Unidad de Geología Regional, Servicio Nacional de Geología y Minería (Sernageomin). Av. Santa María 104, Santiago, Chile. jose.naranjo@sernageomin.cl

[3]Department of Earth, Geographic, and Climate Sciences, University of Massachusetts, Amherst, MA 01003, United States. cailey@umass.edu

[4]Instituto de Ciencias de La Tierra, Facultad de Ciencias, Universidad Austral de Chile, 5090000, Valdivia, Chile. alexandre.corgne@uach.cl

[5]Department of Earth and Environmental Sciences, The University of Manchester, Williamson Building M13 9PL, Manchester, United Kingdom. lewis.hughes@manchester.ac.uk

[6]Carrera de Geología, Facultad de Ingeniería, Universidad Andrés Bello Campus República - Sede Santiago, Sazié 2119, Santiago, Chile. cfelram@gmail.com

ABSTRACT

Ignimbrites are among the largest, and more extensive products of explosive volcanic eruptions on Earth. They are often associated with caldera-forming volcanic events, meaning that characterising their sources remains a fundamental task for understanding crustal magmatism in volcanic arcs. Mainly, since they may represent long-lived polygenetic volcano-magmatic systems. The Altiplano-Puna Volcanic Complex (APVC) is one of the largest areas of silicic magmatism on Earth, concentrating several calderas and large ignimbrite sheets since the late Miocene. In this contribution we describe the general features of the Tálar Caldera and its most likely products, based on morphostratigraphic relationships and literature review. The caldera erupted through Miocene volcanics within a complex system of regional conjugate transtensional structures and forms a 29×20 km depression (~114 km^3 volume). The resulting ~2.5 Ma Tucúcaro and Patao ignimbrites together equate to ~53 km^3 of deposits. After the caldera eruptions, monogenetic and polygenetic Pliocene to recent volcanoes have occupied both the caldera floor and its structural rim. The remaining depression hosts an oblong resurgent dome, 200 m high and ~60 km^2 in area, surrounded by a central moat hosting the Tálar and Capur salt flats. We suggest the Tálar Caldera represents the southernmost recognised caldera of the APVC, and their products offer new insights into the boundary conditions of such massive magmatic bodies. This study provides further background information to understand the complex evolution of superimposed Central Andean volcanic systems and the volcanic activity within the APVC.

Keywords: Ignimbrite, caldera, tuff, geomorphology, rhyolite, APVC, Central Andes.

La caldera de Tálar y sus productos volcánicos: el centro ignimbrítico más meridional del Complejo Volcánico Altiplano-Puna (Andes Centrales). Las ignimbritas se encuentran entre los productos de mayor tamaño y extensión de las erupciones volcánicas explosivas en la Tierra. A menudo se asocian con eventos volcánicos que dan lugar a la formación de calderas, lo que significa que la caracterización de sus orígenes sigue siendo una tarea fundamental para comprender el magmatismo cortical en los arcos volcánicos. Sobre todo, porque pueden representar sistemas volcano-magmáticos poligénicos de larga duración. El Complejo Volcánico Altiplano-Puna (CVAP) es una de las áreas más extensas de magmatismo silícico de la Tierra, donde se concentran varias calderas y grandes ignimbritas desde el Mioceno Tardío. En esta contribución se describen las características generales de la caldera de Tálar y sus productos más probables, con base en relaciones morfoestratigráficas y en una revisión de la literatura. La caldera se emplazó en rocas volcánicas miocenas dentro de un complejo sistema de estructuras transtensionales conjugadas regionales y forma una depresión de 29×20 km con un volumen de ~114 km³. Las ignimbritas resultantes de Tucúcaro y Patao (~2,5 Ma) totalizan un volumen de ~53 km³. Tras las erupciones de la caldera, volcanes monogenéticos y poligenéticos de edades pliocenas a recientes han ocupado tanto el fondo de la caldera como su borde estructural. La depresión restante alberga un domo resurgente oblongo, de 200 m de altura y ~60 km² de superficie, rodeado por un foso central que alberga los salares de Tálar y Capur. Se sugiere, por lo tanto, que la caldera de Tálar constituye la caldera más meridional reconocida para el CVAP, y que sus productos aportan nuevos conocimientos sobre las condiciones de borde en este tipo de cuerpos magmáticos de gran tamaño. Este estudio ofrece información adicional para comprender la compleja evolución de los sistemas volcánicos superpuestos de los Andes Centrales y la actividad volcánica dentro del CVAP.

Palabras clave: Ignimbrita, caldera, toba, geomorfología, riolita, CVAP, Andes Centrales.

1 Introduction

Calderas are wide topographic basins surrounded by an elevated topographic rim resulting from the subvertical collapse of a large area of ground toward a partly drained magma reservoir during large explosive or effusive eruptions (Branney and Acocella, 2015, and references therein). When explosive, these eruptions (≥100 km^3 of ejecta; VEI 7) produce regionally extensive pyroclastic deposits derived from buoyant eruption columns, ground-hugging pyroclastic density currents, and buoyant co-density current clouds. Deposits that fall out from buoyant clouds are known as fall deposits and those from density currents are known as ignimbrites. Some of the most voluminous records of explosive volcanism on Earth are extensive ignimbrite plateaux like the Altiplano-Puna Volcanic Complex (APVC, Central Andes) where regionally extensive ignimbrite sheets, and large, complex, multi-cyclic calderas have formed as the result of a 10-1 Ma ignimbrite flare-up (de Silva et al., 2006). In the APVC, factors such as changing subduction geometry, crustal thickening, oceanic ridge subduction, and crustal delamination may have driven major shifts in volcanic activity since the Late Miocene (Isacks, 1988; de Silva, 1989a; Coira et al., 1993; Coira and Kay, 1993; Kay et al., 1994; Salisbury et al., 2011). Large silicic ignimbrite flare-ups represent the most voluminous volcanic manifestations of this region during this period (e.g., Francis et al., 1989; de Silva, 1989a, b; de Silva and Francis, 1991; Stern, 2004; de Silva et al., 2006; González et al., 2009; Salisbury et al., 2011; Petrinovic et al., 2021; Paine and Wadsworth, 2025). However, not all these massive eruptions (i.e., few 10^2-10^3 km^3) and their sources have been fully characterised to date.

Two superimposed ignimbrites, Tucúcaro (TI) and Patao (PI) (Ramírez and Gardeweg, 1982), are located at the southernmost region of the APVC (Fig. 1). According to previous studies, TI is distributed towards the west of Cosor volcano and in the surroundings of Toloncha volcano (Fig. 1), covering ~600 km^2 with thicknesses of up to 20 m (average thickness of 10-20 m), with its thickest exposures at the bottom of the valleys. Similarly, PI extends over 490 km^2 with a maximum thickness of 30 m (Fig, 1). Both units consist of white to light-brown, grey, and brown-pink moderately welded to welded dacitic tuff, containing planar or fibrous pumice fragments, scarce lithics, and 5-15 vol.% phenocrysts (plagioclase, biotite, K-feldspar, clinopyroxene, hornblende, and quartz) (Álvares-Amado et al., 2022). Both ignimbrites have retrieved similar K-Ar (biotite) ages of 3.2±0.3 (TI) and 3.1±0.7 Ma (PI), however with large errors of 14.3% and 8.3%, respectively (Ramírez and Gardeweg, 1982; Gardeweg and Ramírez, 1985), while $^{40}Ar/^{39}Ar$ dating in plagioclase by Barquero-Molino (2003) and Brown et al. (2021) provided more precise isochron ages for the PI: 2.43±0.03 and 2.54±0.06 Ma, respectively, ages that are preferred in this article. Beyond these chronostratigraphic constraints, their source has not yet been identified. Barquero-Molino (2003) and de Silva and Gosnold (2007) proposed PI was likely sourced south of La Pacana Caldera, while Ramírez and Gardeweg (1982) pointed out the source of TI somewhere at Pampa de Tunco (Fig. 2A). In this contribution, we present new evidence for the existence of a large, hitherto undiscovered caldera structure in the Altiplano-Puna region of Chile, named herein as Tálar Caldera. Combined with new geochemical data, our work also implies that Tálar is the most likely source of the TI and PI ignimbrites and so reconciles long-standing uncertainties over their ultimate source.

2. Methods

2.1 Geomorphologic description

Remote sensing imagery has considerably favoured the finding of undiscovered calderas in the Central Andes since the seminal studies of Francis and Baker (1978) and Baker (1981). We followed the procedure of Branney and Acocella (2015) to identify a potential caldera: 1) recognition of a topographic depression using remote imaging and ©Google Earth™ (see regional satellite image in Supporting Material); 2) ground truth (field) verification of thick, ponded caldera-fill deposits in a down-dropped area surrounded by a structural margin of similar age; 3) identification of proximal volcanic products and peripheral extensive outflow sheets or fans by combining remote sensing with field work; and 4) recognition of the caldera-forming eruption sequence within these deposits. The initial insights on the location of this caldera structure were made by Ramírez and Gardeweg (1982), Barquero-Molino (2003), and de Silva and Gosnold (2007), and served as a starting point for our search.

2.2 Fieldwork, sampling, and whole-rock geochemistry

A field campaign was carried out between February and March 2019 to perform stratigraphic observations of field exposures, mainly along truck traces on the southeastern border of the Salar de Tálar. Field-based geological mapping was complemented with Sentinel 2 RGB satellite imagery with band combinations 4:3:2 and 3:2:1, and the interpretation of ©Google Earth™ imagery. These observations allowed us to recognize, describe, characterise, and map the geomorphology of the caldera and the remnants of its related ignimbrites (Figs. 1 and 2A). We studied the PI rock samples collected and analysed by Brown et al. (2021), that correspond to drilled cores (2.54 cm in diameter, ~10 cm long) near the eastern side of Salar de Atacama, and along Route 23 (Fig. 1). Sampling sites were spread over ~4 meters along

the outcrop. These samples (AT19-124, AT20-134, AT26-180, AT50-388, and AT50-394) were analysed by whole-rock X-Ray fluorescence at the Ronald B. Gilmore Laboratory within the Department of Geosciences at the University of Massachusetts in 2024. Major element data to compare and distinguish TI from PI (Si, Ti, Al, Fe, Mn, Mg, Ca, Na, K, and P) were obtained on a PANalytical Zetium Ultimate, whereas trace elements (Nb, Zr, Y, Sr, U, Rb, Th, Pb, Ga, Zn, Ni, Cr, and V) were measured on pressed powder pellets using a Siemens SRS-1 sequential spectrometer. Standards used were BHVO-2 (Hawaiian Volcano Observatory Basalt) and QL1-A (Oregon Quartz Latite). Average analytical totals of 20 runs on the five samples ranged between 98.33 and 99.0 wt.%. The analytical error of this instrument was better than 10% for major elements and generally better than 20% for trace elements. Supporting Material contains field pictures of different sites where the ignimbrites are visible in the field.

2.3 Petrography and mineral chemistry

Thin sections from samples AT19, AT20 and AT50 were studied with both optical and electron microscopy. Optical microscopy was performed using a Nikon Eclipse polarising microscope. Electron microscopy was performed at the Department of Earth and Environmental Sciences, University of Manchester, using an FEI/Thermofisher Quanta 650 FEG-ESEM equipped with a Bruker XFlash 6|30 energy dispersive X-Ray spectrometer (EDS) paired with ESPRIT software v2.5. We also studied three thin sections: CMBA_A, CMBE_B and CMBS of the Cerro Negro volcano (see location in figures 1 and 2A), which corresponds to one of the post-caldera volcanoes and lies on the southern rim of the caldera. The Cerro Negro rocks were texturally and compositionally studied to be compared to the ignimbrites. The full context, whole-rock geochemistry, and mineralogy of these andesitic

scoria and spatter are provided in Romero et al. (2022). We collected 75 backscattered electron images (BSE) and, where possible, acquired full standards-based quantitative EDS data from mineral phases and glass. Analytical conditions were 15 kV accelerating voltage and 2 nA beam current, with a 5 μm defocused beam to limit the potential for both beam damage and volatile element migration during counting, especially in the case of the glass analyses. Due to poor spectral resolution caused by the surface's flatness and peak-to-background ratios in EDS, spectra were collected for a minimum of 2,000,000 X-Rays to ensure statistically meaningful data and to achieve high accuracy and precision, particularly for minor and trace elements. The analytical setup resulted in count times of ~50 s per data point. Analytical standards used were those available at the FEG-ESEM facility: Jadeite (Na), Anorthite (Si, Ca), Apatite (P), Pyrite (S), Orthoclase (K), Rutile (Ti), Cr_2O_3 (Cr), Tephroite (Mn), Fayalite (Fe), and NiO (Ni). The setup was checked both pre- and post-analysis, and at intervals between these two steps, using well-known and characterised National Museum of Natural History (NMNH) standards. Relative errors (1σ) were <0.5 wt.% for major elements and <10 wt.% for minor elements.

3. Results

3.1 Geomorphology

Combining field and satellite-based evidence, we identify an elongated, oval-shaped depression with a 29 km NNE-SSW long axis by 20 km-width, located immediately south of Miñiques and Tuyajto volcanoes (Fig. 1). Among its characteristic features, we recognise an irregular scarp forming a rim, with an average height of 560 m to the N and 330 m to the NE (Fig. 2B). To the ESE, in Alto Tetera Mocha, its arcuate scarp is ~670 to 700 m high, being

relatively continuous along 24 km approximately N-S (Fig. 2A, B, C). This segment of the rim is partially buried by stepped normal fault planes N40-60°E/50-60°NW. These faults cut biotite-hornblende bearing andesitic lavas, lapilli tuffs and epiclastic breccia units, some of them hosting hydrothermal and phreatic breccias. These volcanic rocks have returned ages of 7.8-5.8 Ma according to whole-rock K-Ar dating (Mirasol Resources Ltd., 2018). To the S and SW, the caldera rim is roofed by the Capur and Tálar volcanoes (Fig. 2A), while the discontinuous scarp to the W and NW is comparatively modest, between 300 and 560 m. Several other discontinuous scarps are observed between Hipiras and Cosor volcanoes (Fig. 2D).

Approximately at the centre of the depression, we recognize a 10×6 km oval structure with a N-S orientation, reaching approximately 200 m above the depression floor **(**Fig. 2B, E). It contains subparallel N24-30°E trending normal faults affecting relicts of PI, with planes dipping ~40-60° and configuring an extensional suite from which the central block is the footwall, producing fault scarps 30-40 m high. As these fault scarps extend below Murchota and Caichinque volcanoes, they likely controlled the formation of both on its northern side. The southern lavas of Caichinque volcano are partially channelled to the south along this extensive structure (Fig. 2A). The central bulge within the depression is surrounded by the Tálar and Capur salt flats. The depression also hosts several Pleistocene to Holocene volcanoes which erupted following the caldera formation (Fig. 2E). One of them is the Cerro Negro cone mentioned above, built on the southern portion of the rim (Romero et al., 2022; Fig. 2A).

The depression, as measured from the rim, has an area of ~310 km^2 (Table 1), whereas its floor covers 205 km^2. Thus, considering an average area of 257 km^2 and a mean depth of 460 m, the estimated depression volume is ~114 km^3.

3.2 Ignimbrite units

The TI outcrops are found up to 70 km WNW of the caldera centre, between elevations of ~4,300 and ~2,300 m a.s.l. in the southern end of the Salar de Atacama. In contrast, PI is distributed up to 50 km NW of the caldera centre, at ~2,400 m a.s.l., and to the east between 15 and 25 km at elevations between ~3,800 and ~4,200 m a.s.l. (Fig. 1). This dominant W-trending disposition is mostly controlled by the steep topography of the Central Andean plateau in this area and its limited outcrops towards the east probably reflect the burial of these ignimbrites beneath younger volcanic products. The lack of natural outcrops with sufficient depth prevents direct observation of the TI within the depression (Ramírez and Gardeweg, 1982), meaning that only the PI is exposed (Fig. 2A). Distal remains of the TI are observable to the west at the basal part of the Tilocálar volcanoes (Ureta et al., 2020). Both ignimbrites become thinner towards the N, S and W from the area around Caichinque volcano.

In the northern side of Salar de Tálar, the minimum PI thicknesses vary from 10 to 15 m (base not observed). It shows a vertical gradation from the lower unwelded pumice-rich, light grey or brown region to a highly welded dark brown to dark grey top (Fig. 3A, B), also bearing abundant (5-15%) reversely graded fiamme. The largest pumices are 5-10 cm in diameter. This vertical gradational change in colour and texture is accompanied by sharp contact surfaces that reflect the superposition of continuous pyroclastic density current layers

composing this thick deposit unit (Fig. 3B). Scarce PI outcrops have been identified ~5 km NNE from the CNV at elevations between 4,200 and 4,500 m a.s.l., where narrow ravines reveal a massive, brecciated deposit reaching ~55 m thickness (Fig. 3C) and thick remnants up to 125 m in height (Fig. 3D), thus suggesting a maximum observed thickness in this locality. To the N side of the Tálar Caldera, the PI is directly overlain by the Middle Pleistocene Tuyajto Ignimbrite (Brown et al., 2021), which is 1 to 3 m thick, with a reddish and massive aspect, and upward welding (Fig. 3E), locally developing a conspicuous columnar jointing. Towards the west, the ignimbrites form a plateau (Fig. 3F), which is locally covered in erosive contact by Quaternary alluvial deposits (Fig. 3G). In the central parts of the depression, all ignimbrite exposures are present but the bulge, which is buried beneath alluvial sedimentary deposits and aeolian sands (Fig. 3H).

3.3 Petrography and geochemistry

In hand specimens of both PI and TI ignimbrites, the samples are very similar and correspond to grey, welded, crystal- and pumice-poor tuffs. They contain a fine-grained ash matrix with angular quartz and blocky plagioclase up to 2 mm in size, hornblende laths, acicular pyroxene and fine-grained biotite. Lithics are scarce and they reach up to 3 mm in size. At the microscale, both ignimbrites correspond to vitric tuffs with crystals. The TI consists of 74% glass and 26% crystals, with dominant plagioclase (21%), biotite (4%) and amphibole (1%). Comparatively, the PI contains 64-84% glass and 16-36% crystals, which correspond to plagioclase (10-19%; Fig. 4A), quartz (1-8%; Fig. 4B), biotite (1-4%; Fig. 4C), amphibole (1-3%; Fig. 4D), orthopyroxene (2%), and clinopyroxene (1%) (Fig. 3E). Lithics only

represent 1% (Fig. 4F). In these units, the normalised glass is represented by variable abundance of shards (64-74%), fine ash matrix (15-39%), and pumices (1-9%).

Whole-rock geochemistry (Table 1) based on bulk matrix samples indicates that the PI tuffs are rhyolitic (70.8-72.5 wt.% SiO_2; Fig. 5A), belonging to the high-K (3.6-4.0 wt.% K_2O; Fig. 5B) and high-alkali calc-alkaline series (8.2-8.6 wt.% Na_2O+K_2O; Fig. 5C). These products are slightly less evolved than the TI tuff samples analysed by Ureta et al. (2022) (Fig. 5A, B, C), which also correspond to high-K (4.6-4.8 wt.% K_2O) rhyolites (74.7-75.1 wt.% SiO_2). Both ignimbrites' trace element patterns are very similar, except for a less pronounced Sr negative anomaly in the PI (Fig. 5D). The TI ignimbrite shows a somewhat higher degree of differentiation given the slightly higher contents in incompatible elements (Rb, U, Th, and K) and higher Zr/Ti and Zr/V ratios (13-15.5 and 834-1,014, respectively). Its higher Sr anomaly (193-262 ppm) and lower Al (7.45-8.0 wt.%), Ca (1.2-2.0 wt.%), and Na (3.2-3.6 wt.%) contents probably indicate that its parental magma experienced more plagioclase fractionation. REE patterns obtained by Kay et al. (2010) and Ureta et al. (2020) are nearly identical and support the chemical similarity between the two deposits. The PI and TI ignimbrites also show similar trace element patterns to the nearby <4.5 Myr Toconao, Purico and Atana ignimbrites, particularly with the latter (de Silva, 1991; Lindsay et al., 2001; Salisbury et al., 2011). The similarities with rock compositions presented by Kay et al. (2010) may highlight a common chemical signature shared by these products related to the APVC magma body (Fig. 5D). Although small differences can be observed. Their La/Yb are slightly lower (5.2, 12.1-18.1, and 15.2, respectively) than the values obtained for the PI and

TI ignimbrites (18.1 and 19.1, respectively). Moreover, the chondrite-normalised Th/U ratio is <1 (0.5-0.8) for the nearby ignimbrites but >1 (1.2-1.3) for the PI and TI ignimbrites.

4. Discussion

Previously, de Silva and Gosnold (2007) suggested the source of the PI was unknown but likely somewhere to the south of La Pacana caldera. Additionally, Ramírez and Gardeweg (1982) had proposed the source of the TI somewhere at Pampa de Tunco, a few kilometres west from the depression described in this contribution. We interpret the above-described geomorphology as the newly Tálar Caldera (Figs. 1 and 2; Table 2), and its central bulge as a resurgent dome with its associated apical graben. Given their proximity, stratigraphic correspondence, and radial thinning, we now consider both the TI and PI as potentially sourced from this caldera (Table 2).

Estimating the volume of these ignimbrites is challenging, given their complex distribution, post-depositional erosive processes, and restricted exposure within the caldera. A very conservative volume can be obtained following the Salisbury et al. (2011) approach. These authors recommended considering the maximum relief between the resurgent intracaldera domes and their surrounding moats as the minimum thickness of the intracaldera ignimbrite to obtain an intracaldera ignimbrite volume. Thus, considering the exposed area of the resurgent block and its maximum relief, we estimate an intracaldera volume of 15.8 km^3 (51.6 km^2 and 306 m above the floor). This volume only considers PI, as TI remains obscured by PI and caldera floor sediments. On the other hand, the outflow quantification was obtained by using the total extra-caldera areal extent of these ignimbrite outcrops and their average thickness based on the approach of Salisbury et al. (2011). By using the envelope of all the

outcrops to approximate the total uneroded deposit extent, the resulting volumes are 23 km^3 and 30 km^3 for the Tucúcaro and Patao ignimbrites, respectively (TI ~1500 km^2 and PI ~1500 km^2). These estimates account for ~53 km^3, or ~40 km^3 (DRE) assuming a density in the range of 1.8-2.2 g/cm^3, that means a DRE volume of ~75% of its bulk counterpart (Salisbury et al., 2011). These volumes are comparable the total erupted products of the historical Novarupta-Katmai (1912) eruption in Alaska (e.g., Hildreth and Fierstein, 2012), or the ignimbrite volume released by the 7.7 ka Mount Mazama eruption in the United States (Druitt and Bacon, 1986; Buckland et al., 2020). The bulk volume accounts for as much as 46% of the total depression volume (~114 km^3), meaning that the remaining volume, if any, is probably buried beneath younger eruptive centres or has been eroded. Volcanic products from the exterior of the caldera also occupy its floor, including the Quaternary Miñiques, Tuyajto, Capur, and Tálar volcanoes (Fig. 2A). The limited vertical exposure of both the TI and PI in the proximal areas of the Tálar Caldera does not allow identifying their lowermost eruptive units, including the basal pumice tephra fallout, the heterolithic breccias, and the co-ignimbrite and post-collapse fallouts, which were likely eroded or buried beneath the moat deposits. Therefore, the calculated volumes for the PI and TI should be considered as conservative, minimum estimates. These volumes are comparable to those of other APVC ignimbrites reported in Salisbury et al. (2011), such as the ~0.7 Ma Tatio (52.8 km^3) and the ~5.2 Ma Alota (29 km^3) ignimbrites. The moat deposits may have originated by a complex interplay between tectonic subsidence and fluctuating arid climatic conditions with infrequent pluvial events (e.g. Valero-Garcés et al., 1999; Amundson et al., 2012).

The Tálar Caldera lies at the intersection of NE- and NW-trending volcanic lineaments, related to faults with sinistral and dextral displacements, respectively (Strecker et al., 1989;

Chernicoff et al., 2002; Richards and Villeneuve, 2002). It is also influenced by compressive structures to the west (e.g., Miscanti Fault; Fig. 2A) which are related to regional E-W shortening (Allmendinger et al., 1983) since around 10 Ma (e.g., Riller et al., 2001; Matteini et al., 2002; Norini et al., 2013). More recently, the development of coeval contractional and extensional structures of regional importance between 2.4 and 0.7 Ma is interpreted as induced by orogen collapse (Tibaldi and Bonali, 2016). In this sense, orogenic collapse together with conjugate transtensional structures may have created conditions for large magma volumes to ascend and evolve, then favouring the occurrence of caldera volcanism. Similar geodynamic settings are described by Naranjo et al. (2018) for the Salar Grande, Barrancas Blancas and Pampa de los Bayos calderas, ~250 km south of our study area, which can explain the accumulation and eruption of large volumes of silicic magmas.

The austral position and modest size of the Tálar Caldera and its deposits, relative to the rest of the APVC ignimbrite flare-up sources, are consistent with the observations of de Silva and Gosnold (2007), who noticed that the ignimbrite flare-up events in the APVC have markedly decreased in intensity during the past 4 Myr (Table 3) and have shifted toward the periphery of the major complexes. Indeed, the location of the Tálar Caldera is peripheral to the surface projection of the Altiplano Puna Magmatic Body (APMB; Prezzi et al., 2009), interpreted as an amalgamated plutonic complex of 200 km diameter and 11 km thick (Ward et al., 2014). The rhyolitic character of the TI and PI ignimbrites are uncommon for the dominantly dacitic APVC ignimbrites, as similarly happens in the rhyolitic Caspana and Chaxas ignimbrites, which are also peripheral to the APMB (e.g., Lewis et al., 2022, 2025). In addition, the development of andesitic volcanoes following the Tálar Caldera formation may tell a story of variations from large-volume silicic volcanism towards the development of the modern,

Quaternary arc after the waning of the thermal influence imposed by the APMB locally (e.g., Burns et al., 2015; Lewis et al., 2025).

Considering the very narrow radiometric age ranges reported for the PI and TI (e.g., Ramírez and Gardeweg, 1982; Gardeweg and Ramírez, 1985; Barquero-Molino, 2003; Brown et al., 2021), and their significant petrographic and compositional similarities highlighted by our analysis, we posit that both units might correspond to two phases of the same event, or two successive eruptions shortly spaced in time, as it has been observed in other APVC ignimbrites and elsewhere (e.g., Hildreth, 1981; Dunbar et al., 1989; Wallace et al., 1999; Lindsay et al., 2001; Bachmann and Bergantz, 2008; Masotta et al., 2010; Cashman et al., 2017; Grocke et al., 2017; Wilson et al., 2021). This observation warns of a potential "dual-event scenario" that could have profound implications for volcanic hazard and risk during large-explosive scale eruptions. To establish their co-genetic and spatial and temporal relationships, we encourage further research, including detailed stratigraphic, geochronological, petrological, and geochemical studies on these products.

Recognising the existence of a new, southernmost caldera related to the APVC and its respective explosive deposits offers a new opportunity to better understand the cycles of ignimbrite flare-up events that interrupt steady-state volcanism in active volcanic arcs (e.g., Bertin et al., 2023). Therefore, our contribution adds new background information on the boundary conditions of one of the largest and most studied silicic magma bodies in the world (e.g., de Silva, 1989a; Francis et al., 1989; Salisbury et al., 2011).

5. Conclusions

In this work, we present new evidence for the existence of a previously unrecognized caldera in the Central Andes, constituting the southernmost ignimbrite flare-up manifestation of the large felsic Altiplano Puna Volcanic Complex (AVPC). The Tálar Caldera is 29×20 km in size, with an estimated depression volume of ~114 km^3. The formation of this caldera seems to have been controlled by the interplay between the collapse of the Central Andean orogen and regional conjugate transtensional structures, which allowed large volumes of magmas to ascent and evolve. We propose that this caldera is the most probable source of the Tucúcaro and Patao rhyolitic ignimbrites (~2.5 Ma). The minimum estimated bulk volume of these two ignimbrites equates to 53 km^3, equivalent to 40 km^3 DRE. We propose that these ignimbrites may represent two phases of the same event or two successive eruptions closely spaced in time. The location of the caldera and the compositional and mineralogical features of these ignimbrites can provide valuable information on the boundary conditions of the magma body that underlies the APVC.

Acknowledgements

We appreciate the discussion and support of M. Cáceres Munizaga and P. Fuentes Molina in a previous stage to this research. We thank M. Gardeweg by discussing some of the aspects of this contribution with us. The support of C. Condit during paleomagnetic coring and lithological description is appreciated. The reviews provided by S. de Silva, A. Paine, and M. Villarroel significantly improved the quality of this work. This is a contribution to the Plan Nacional de Geología (PNG) of the Servicio Nacional de Geología y Minería (Chilean National Geology and Mining Survey), Chile (JAN).

Supporting Material can be accessed in the following link https://doi.org/10.6084/m9.figshare.32012472

References

Allmendinger, R.W.; Jordan, T.E.; Kay, S.M.; Isacks, B.L. 1997. The evolution of the Altiplano-Puna plateau of the Central Andes. Annual Review of Earth and Planetary Sciences, 25(1): 139-174. 10.1146/annurev.earth.25.1.139

Allmendinger, R. W.; Ramos, V. A.; Jordan, T. E.; Palma, M.; Isacks, B. L. 1983. Paleogeography and Andean structural geometry, northwest Argentina. Tectonics, 2(1), 1-16.

Amundson, R.; Dietrich, W.; Bellugi, D.; Ewing, S.; Nishiizumi, K.; Chong, G.; Owen, J.; Finkel, R.; Heimsath, A; Stewart, B; Caffee, M. 2012. Geomorphologic evidence for the late Pliocene onset of hyperaridity in the Atacama Desert. Bulletin, 124(7-8), 1048-1070.

Bachmann, O.; Bergantz, G. W. 2008. Deciphering Magma Chamber Dynamics from Styles of Compositional Zoning in Large Silicic Ash Flow Sheets. Reviews in Mineralogy and Geochemistry, 69(1), 651–674. https://doi.org/10.2138/RMG.2008.69.17

Báez, W.; Arnosio, M.; Chiodi, A.; Ortiz-Yañes, A.; Viramonte, J. G.; Bustos, E.; Guiordano, G.; López, J. F. 2015. Estratigrafía y evolución del Complejo Volcánico Cerro Blanco, Puna Austral, Argentina. Revista mexicana de ciencias geológicas, 32(1), 29-49.

Baker, M.C.W. 1981. The nature and distribution of upper Cenozoic ignimbrite centers in the Central Andes. Journal of Volcanology and Geothermal Research, 11(2-4), 293-315.

Barquero-Molino, M. 2003. 40Ar/39Ar chronology and paleomagnetism of ignimbrites and lavas from the Central Volcanic Zone, northern Chile, and 40Ar/39Ar chronology of

silicic ignimbrites from Honduras and Nicaragua. MS Thesis, University of Wisconsin, 70 pp.

Bertin, D.; de Silva, S.L.; Lindsay, J.M.; Cronin, S.J.; Caffe, P.J.; Connor, C.B.; Grosse, P.; Báez, W.; Bustos, E.; Constantinescu, R., 2023. Magmatic addition rates differentiate periods of steady-state versus flare-up magmatism in the Central Andean arc. Commun Earth Environ 4, 75. https://doi.org/10.1038/s43247-023-00744-2

Branney, M.; Acocella, V. 2015. Calderas. In The encyclopedia of volcanoes. The Encyclopedia of Volcanoes (Second Edition). Academic Press, Amsterdam, pp. 299-315.

Brown, L.; Singer, B.S.; Barquero-Molina, M. 2021. Paleomagnetism and 40Ar/39Ar chronology of ignimbrites and lava flows, Central Volcanic Zone, Northern Chile. Journal of South American Earth Science, 106: 103037. https://doi.org/10.1016/j.jsames.2020.103037

Buckland, H. M.; Cashman, K. V.; Engwell, S. L.; Rust, A. C. 2020. Sources of uncertainty in the Mazama isopachs and the implications for interpreting distal tephra deposits from large magnitude eruptions. Bulletin of Volcanology, 82(3), 23.

Burns, D.H.; de Silva, S.L.: Tepley, F.; Schmitt, A.K.; Loewen, M.W., 2015. Recording the transition from flare-up to steady-state arc magmatism at the Purico- Chascon volcanic complex, northern Chile: Earth and Planetary Science Letters, v. 422, p. 75–86, https://doi.org/10.1016/j.epsl.2015.04.002.

Cashman, K.V.; Sparks, R.S.J.; Blundy, J.D. 2017. Vertically extensive and unstable magmatic systems: A unified view of igneous processes. Science 355, eaag3055. DOI:10.1126/science.aag3055

Chernicoff, C. J.; Richards, J. P.; Zappettini, E. O. 2002. Crustal lineament control on magmatism and mineralization in northwestern Argentina: geological, geophysical, and remote sensing evidence. Ore Geology Reviews, 21(3-4), 127-155.

Coira, B.; Kay, S. M. 1993. Implications of Quaternary volcanism at Cerro Tuzgle for crustal and mantle evolution of the Puna Plateau, Central Andes, Argentina. Contributions to Mineralogy and Petrology, 113(1): 40-58. 10.1007/BF00320830

Coira, B.; Kay, S. M.; Viramonte, J. 1993. Upper Cenozoic Magmatic Evolution of the Argentine Puna—a Model for Changing Subduction Geometry. International Geology Review, 35(8): 677-720. 10.1080/00206819309465552

de Silva, S. L.; Gosnold, W. D. 2007. Episodic construction of batholiths: Insights from the spatiotemporal development of an ignimbrite flare-up. Journal of Volcanology and Geothermal Research, 167(1-4), 320-335.

de Silva, S.L. 1989a. Altiplano-Puna volcanic complex of the central Andes. Geology, 17(12): 1102-1106.

de Silva, S.L. 1989b. Geochronology and stratigraphy of the ignimbrites from the 21°30′S to 23°30′S portion of the Central Andes of northern Chile. Journal of Volcanology and Geothermal Research, 37(2): 93-131. https://doi.org/10.1016/0377-0273(89)90065-6

de Silva, S.L.; Francis, P.W. 1991. Volcanoes of the central Andes. Springer-Verlag, Berlin.

de Silva, S.; Zandt, G.; Trumbull, R.; Viramonte, J. 2006. Large-scale silicic volcanism—The result of thermal maturation of the crust. Advances in Geosciences: Volume 1: Solid Earth (SE), 215-230.

Druitt TH, Bacon CR (1986) Lithic breccia and ignimbrite erupted during the collapse of Crater Lake Caldera, Oregon. J Volcanol Geotherm Res 29:1–32. https://doi.org/10.1016/0377-0273(86)90038-7

Dunbar, N. W.; Kyle, P. R.; Wilson, C. J. N. 1989. Evidence for limited zonation in silicic magma systems, Taupo Volcanic Zone, New Zealand. Geology, 17(3), 234. https://doi.org/10.1130/0091-7613

Francis, P.W.; Baker, M.C.W. 1978. Sources of two large ignimbrites in the central Andes: some Landsat evidence. Journal of Volcanology and Geothermal Research, 4(1-2), 81-87.

Francis, P.W.; R. S. J. Sparks, C.J.; Hawkesworth, R. S.; Thorpe, D. M.; Pyle, S. R.; Tait, M. S. Mantovani; McDermott, F. 1989. Petrology and geochemistry of volcanic rocks of the Cerro Galan caldera, northwest Argentina. Geological Magazine, 126(5): 515-547. 10.1017/S0016756800022834

Gardeweg, M.; Ramírez, C.F. 1985. Hoja Rio Zapaleri. II Region de Antofagasta. Escala 1: 250.000.

González, G., Cembrano, J.; Aron, F.; Veloso, E.E.; Shyu, J.B.H. 2009. Coeval compressional deformation and volcanism in the central Andes, case studies from northern Chile (23°S–24°S). Tectonics, 28(6): TC6003. doi:10.1029/2009TC002538

Grocke, S. B.; de Silva, S. L.; Iriarte, R.; Lindsay, J. M.; Cottrell, E. 2017. Catastrophic Caldera-Forming (CCF) Monotonous Silicic Magma Reservoirs: Geochemical and Petrological Constraints on Heterogeneity, Magma Dynamics, and Eruption Dynamics of the 3·49 Ma Tara Supereruption, Guacha II Caldera, SW Bolivia. Journal of Petrology, 58(2), 227–260. https://doi.org/10.1093/PETROLOGY/EGX012

Guzmán, S.; Grosse, P.; Martí, J.; Petrinovic, I.; Seggiaro, R. 2017. Calderas cenozoicas argentinas de la zona volcánica central de los Andes – procesos eruptivos y dinámica: una revisión. En: Muruaga, C.M. y Grosse, P. (Eds.), Ciencias de la Tierra y Recursos

Naturales del NOA. Relatorio del XX Congreso Geológico Argentino, San Miguel de Tucumán: 518-547. ISBN 978-987-42-6666-8

Hildreth, W. 1981. Gradients in silicic magma chambers: Implications for lithospheric magmatism. Journal of Geophysical Research: Solid Earth, 86(B11), 10153–10192. https://doi.org/10.1029/JB086IB11P10153

Hildreth, W.; Fierstein, J. 2012. The Novarupta-Katmai eruption of 1912: largest eruption of the twentieth century: centennial perspectives (p. 259). US Geological Survey.

Irvine, T. N.; Baragar, W. R. A. F. 1971. A guide to the chemical classification of the common volcanic rocks. Canadian journal of earth sciences, 8(5), 523-548.

Isacks, B.L. 1988. Uplift of the Central Andean Plateau and bending of the Bolivian Orocline. J Geophys Res: Solid Earth, 93(B4): 3211-3231. https://doi.org/10.1029/JB093iB04p03211

Kay, S. M.; Coira, B. L.; Caffe, P. J.; Chen, C. H. 2010. Regional chemical diversity, crustal and mantle sources and evolution of central Andean Puna plateau ignimbrites. Journal of Volcanology and Geothermal Research, 198(1-2), 81-111.

Kay, S.M.; Coira, B., Viramonte, J. 1994. Young mafic back-arc volcanic rocks as indicators of continental lithospheric delamination beneath the Argentine Puna Plateau, central Andes. Journal of Geophysical Research: Solid Earth, 99(B12): 24323-24339. doi:10.1029/94JB00896

Lee, SG.; Tanaka, T.; Lee, M.J. 2023. Geochemical implication of Eu isotopic ratio in anorthosite: new evidence of Eu isotope fractionation during feldspar crystallization. Geosci J 27, 271–284 (2023). https://doi.org/10.1007/s12303-023-0009-6

Lewis, C.T.; de Silva, S.L.; Burns, D.H., 2022. Rhyolitic melt production in the midst of a continental arc flare-up—The heterogeneous Caspana ignimbrite of the Altiplano-Puna volcanic complex of the Central Andes. Geosphere. https://doi.org/10.1130/ges02462.1

Lewis, C.; de Silva, S.; Cisneros de Leon, A.; Burns, D.; Villarroel, M., 2025. Effusive volcanic microcosm of a regional ignimbrite flare-up: Prolonged life cycle of the Chaxas Complex, northern Chile, and its influence on modern volcanic arc character. Geol. Soc. Am. Bull. https://doi.org/10.1130/b37909.1

Lindsay, J.M.; Schmitt, A.K.; Trumbull, R.B.; De Silva, S.L.; Siebel, W.; Emmermann, R. 2001. Magmatic evolution of the La Pacana caldera system, Central Andes, Chile: Compositional variation of two cogenetic, large-volume felsic ignimbrites. Journal of Petrology, 42(3), 459-486.

Mamani, M.; Wörner, G.; Sempere, T. 2010. Geochemical variations in igneous rocks of the Central Andean orocline (13 S to 18 S): Tracing crustal thickening and magma generation through time and space. Bulletin, 122(1-2), 162-182.

Masotta, M.; Gaeta, M.; Gozzi, F.; Marra, F.; Palladino, D. M.; Sottili, G. 2010. H_2O- and temperature-zoning in magma chambers: The example of the Tufo Giallo della Via Tiberina eruptions (Sabatini Volcanic District, central Italy). Lithos, 118(1–2), 119–130. https://doi.org/10.1016/J.LITHOS.2010.04.004

Matteini, M.; Mazzuoli, R.; Omarini, R.; Cas, R.; Maas, R. 2002. Geodynamical evolution of Central Andes at 24°S as inferred by magma composition along the Calama–Olacapato–El Toro transversal volcanic belt. Journal of Volcanology and Geothermal Research, 118(1): 205-228. https://doi.org/10.1016/S0377-0273(02)00257-3

Mirasol Resources Ltd. 2018. Altazor Gold Project Update: Mirasol Receives Option Payment as Newcrest Exercises Farm-in Stage of the Altazor Agreement, and Reports Exploration Results from First Season Exploration. Accessed on 7 April 2026.

Naranjo, J. A.; Villa, V.; Ramírez, C.; Pérez de Arce, C. 2018. Volcanism and tectonism in the southern Central Andes: Tempo, styles, and relationships. Geosphere, 14(2): 626-641.

Norini, G.; Baez, W.; Becchio, R.; Viramonte, J.; Giordano, G.; Arnosio, M.; Pinton, A.; Groppelli, G. 2013. The Calama–Olacapato–El Toro fault system in the Puna Plateau, Central Andes: Geodynamic implications and stratovolcanoes emplacement. Tectonophysics, 608: 1280-1297. https://doi.org/10.1016/j.tecto.2013.06.013

Paine, A.R.; Wadsworth, F.B. 2025. Large explosive eruptions may be dominated by pyroclastic flows instead of buoyant plumes: insights from a global data compilation. J Appl. Volcanol. 14, 3. https://doi.org/10.1186/s13617-025-00151-6

Petrinovic, I.A.; Hernando, I.R.; Guzmán, S.R. 2021. Miocene to Recent collapse calderas of the southern and central volcanic zones of the Andes and their tectonic constraints. International Journal of Earth Sciences, 1-36.

Prezzi, C.; Götze, H.-J.; Schmidt, S. 2009. 3D density model of the Central Andes. Phys. Earth Planet. In. 177, 217–234.

Ramírez, C.F. 1978. Geología del cuadrángulo Socaire y sector oriental del cuadrángulo Peine. Prospección y evaluación de elementos polimetálicos, Alta Cordillera, II Región. Etapa 2. Instituto de Investigaciones Geológicas, Santiago, 70 p.

Ramírez, C.F.; Gardeweg, M. 1982. Hoja Toconao, Región de Antofagasta. Instituto Geográfico Militar, Santiago, 122 pp.

Richards, J. P.; Villeneuve, M. 2002. Characteristics of late Cenozoic volcanism along the Archibarca lineament from Cerro Llullaillaco to Corrida de Cori, northwest Argentina. Journal of Volcanology and Geothermal Research, 116(3-4), 161-200.

Riller, U.; Petrinovic, I.; Ramelow, J.; Strecker, M.; Oncken, O. 2001. Late Cenozoic tectonism, collapse caldera and plateau formation in the central Andes. Earth and Planetary Science Letters, 188(3): 299-311. https://doi.org/10.1016/S0012-821X(01)00333-8

Romero, J.E.; Ureta, G.; Fuentes, P.; Corgne, A.; Naranjo, J.A.; Ramírez, C.F.; Chako-Tchamabé, B.; Cáceres, M.; Lazcano, J. 2022. The eruptive history and magma composition of Pleistocene Cerro Negro volcano (Northern Chile): Implications for the complex evolution of large monogenetic volcanoes. Journal of Volcanology and Geothermal Research, 429, 107618.

Salisbury, M.J.; Jicha, B.R.; de Silva, S.L.; Singer, B.S.; Jiménez, N.C.; Ort, M.H. 2011. $^{40}Ar/^{39}Ar$ chronostratigraphy of Altiplano-Puna volcanic complex ignimbrites reveals the development of a major magmatic province. GSA Bulletin, 123(5-6), 821-840.

Schmitt, A.; de Silva, S.; Trumbull, R.; Emmermann, R. 2001. Magma evolution in the Purico ignimbrite complex, northern Chile: evidence for zoning of a dacitic magma by injection of rhyolitic melts following mafic recharge. Contributions to Mineralogy and Petrology, 140, 680-700.

Schnurr, W.B.W.; Trumbull, R.B.; Clavero, J.; Hahne, K.; Siebel, W.; Gardeweg, M. 2007. Twenty-five million years of silicic volcanism in the southern central volcanic zone of the Andes: geochemistry and magma genesis of ignimbrites from 25 to 27 S, 67 to 72 W. Journal of Volcanology and Geothermal Research, 166(1), 17-46.

Stern, C.R. 2004. Active Andean volcanism: its geologic and tectonic setting. Revista geológica de Chile, 31: 161-206.

Strecker, M.R.; Cerveny, P.; Bloom, A.L.; Malizia, D. 1989. Late Cenozoic tectonism and landscape development in the foreland of the Andes: Northern Sierras Pampeanas (26–28 S), Argentina. Tectonics, 8(3), 517-534.

Sun, S. S.; McDonough, W. F. 1989. Chemical and isotopic systematics of oceanic basalts: implications for mantle composition and processes. Geological Society, London, Special Publications, 42(1), 313-345.

Tassara, A.; Götze, H.J.; Schmidt, S.; Hackney, R. 2006. Three-dimensional density model of the Nazca plate and the Andean continental margin. Journal of Geophysical Research: Solid Earth, 111(B9).

Tibaldi, A.; Bonali, F.L.; Pasquaré Mariotto, F.A. 2016. Interaction between transform faults and rift systems: a combined field and experimental approach. Frontiers in Earth Science, 4, 33.

Ureta, G.; Aguilera, F.; Németh, K.; Inostroza, M.; González, C.; Zimmer, M.; Menzies, A. 2020. Transition from small-volume ephemeral lava emission to explosive hydrovolcanism: The case of Cerro Tujle maar, northern Chile. Journal of South American Earth Sciences, 104, 102885.

Valero-Garcés, B. L.; Grosjean, M.; Kelts, K.; Schreier, H.; Messerli, B. 1999. Holocene lacustrine deposition in the Atacama Altiplano: facies models, climate and tectonic forcing. Palaeogeography, Palaeoclimatology, Palaeoecology, 151(1-3), 101-125.

Wallace, P.J.; Anderson, A.T.; Davis, A.M. 1999. Gradients in H2O, CO2, and exsolved gas in a large-volume silicic magma system: Interpreting the record preserved in melt

inclusions from the Bishop Tuff. Journal of Geophysical Research: Solid Earth, 104(B9), 20097–20122. https://doi.org/10.1029/1999jb900207

Ward, K.M.; Zandt, G.; Beck, S.L.; Christensen, D.H.; McFarlin, H. 2014. Seismic imaging of the magmatic underpinnings beneath the Altiplano-Puna volcanic complex from the joint inversion of surface wave dispersion and receiver functions. Earth and Planetary Science Letters, 404, 43-53.

Wilson, C.J.N.; Cooper, G.F.; Chamberlain, K.J.; Barker, S.J.; Myers, M.L.; Illsley-Kemp, F.; Farrel, J. 2021. No single model for supersized eruptions and their magma bodies. Nat Rev Earth Environ **2**, 610–627. https://doi.org/10.1038/s43017-021-00191-7

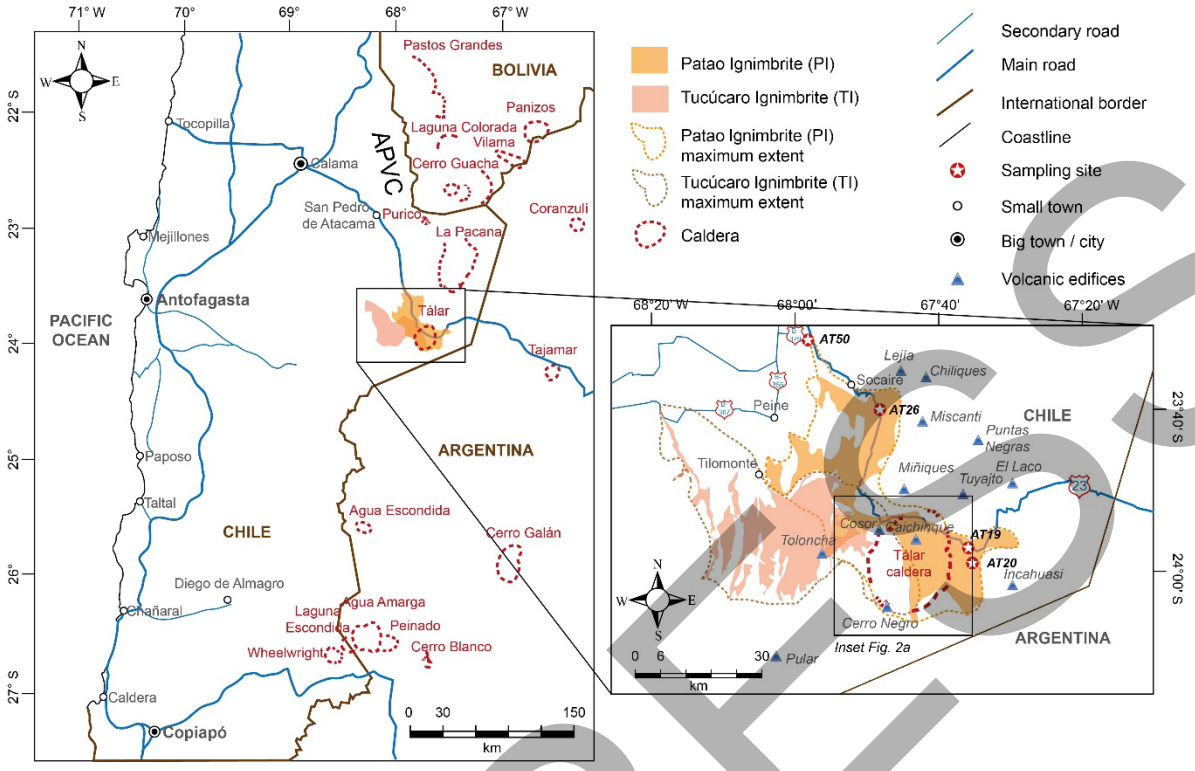

Fig. 1. Location map of the suggested Tálar Caldera and the Patao and Tucúcaro ignimbrites (modified from Ramírez and Gardeweg, 1982). Other calderas from the Altiplano-Puna Volcanic Complex (APVC) and the southern Central Volcanic Zone of the Andes are also indicated (based on Salisbury et al., 2011, Guzmán et al., 2017, Naranjo et al., 2018, and Petrinovic et al., 2021).

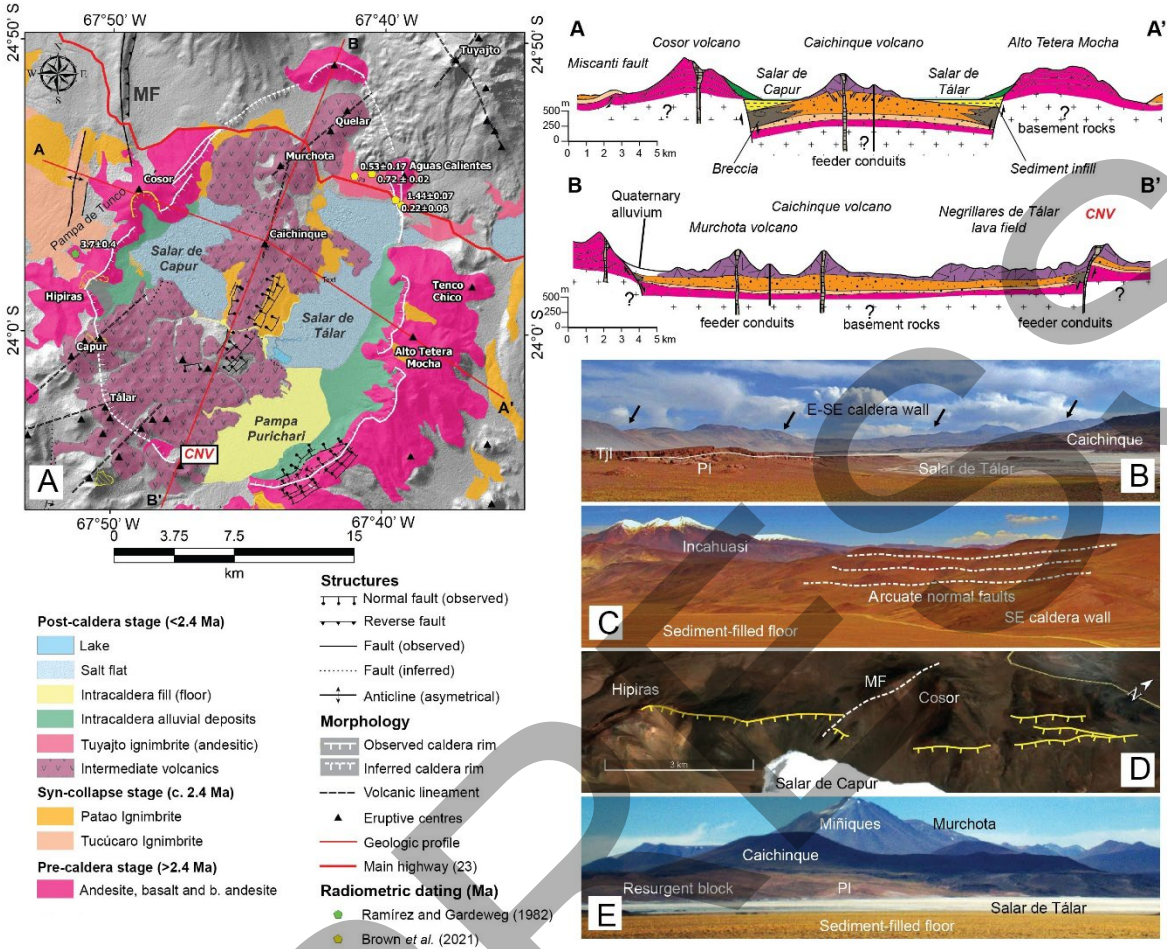

Fig. 2. Geology and geomorphology of the Tálar Caldera. **A.** Geological map, showing the main units, structures, and morphometry elements as well as radiometric ages and neighbouring volcanic centres. Schematic geologic profiles (vertically exaggerated) are shown to the right (see profile traces AA' and BB' on the main map). In these profiles, question marks reflect uncertainty in the geometry of the mapped structures or deposits. Background image: 12.5-m resolution ALOS PALSAR derived shaded relief model (obtained from https://search.asf.alaska.edu/#/). **B.** E-SE caldera wall and intracaldera ignimbrites as observed from the N of Salar de Tálar. **C.** Arcuate normal faults in the SE caldera wall (south of Alto Tetera Mocha) and the caldera fill. **D.** Observed caldera rim between Cosor and Hipiras volcanoes, west of Salar de Capur. Image taken from Google Earth™ (see Supporting Material). **E.** Resurgent block overlaid by Caichinque volcano, between Salar de Tálar and Salar de Capur. Photo by Carolina Pérez. PI: Patao Ignimbrite; TjI: Tuyajto Ignimbrite; CNV: Cerro Negro volcano: MF: Miscanti Fault.

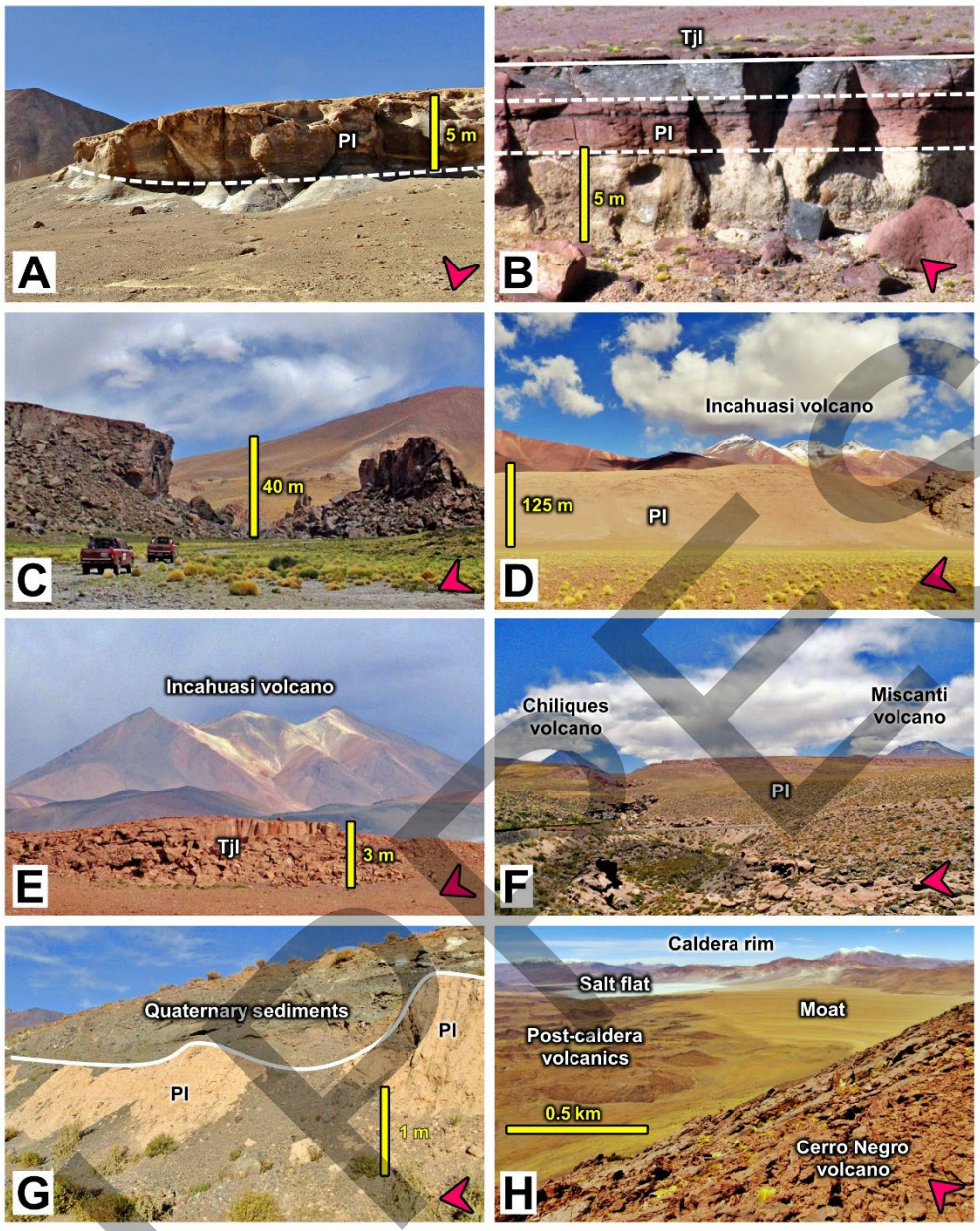

Fig. 3. Ignimbrite deposits associated with the Tálar Caldera. North is indicated with the green arrow. **A-B.** Vertical variations of welding and colour in the Patao Ignimbrite (PI; base not observed), from a lowermost unwelded grey-to-brown region to an uppermost reddish dark brown to dark grey welded region. The Tuyajto Ignimbrite (TjI) is overlying in sharp contact the PI (solid white line). Diffuse contacts are shown with white dashed lines. **C.** Thick exposure (~55 m) of the PI ~5 km NNE from Cerro Negro volcano. **D.** Massive, 125-m thick uneroded relict of the PI, 2 km E from Tenco Chico volcano. **E.** TjI outcrop near Route 23, displaying columnar jointing to its upper half. **F.** Plateau formed by the accumulation of PI at the Nacimiento ravine, near the town of Socaire. **G.** Eroded top of the PI covered by modern alluvial sediments in a roadcut west of Miscanti volcano. **H.** Sedimentary deposits filling the caldera depression (moat) and post-caldera volcanics, covering the ignimbrite exposures. See figure 1 for locations.

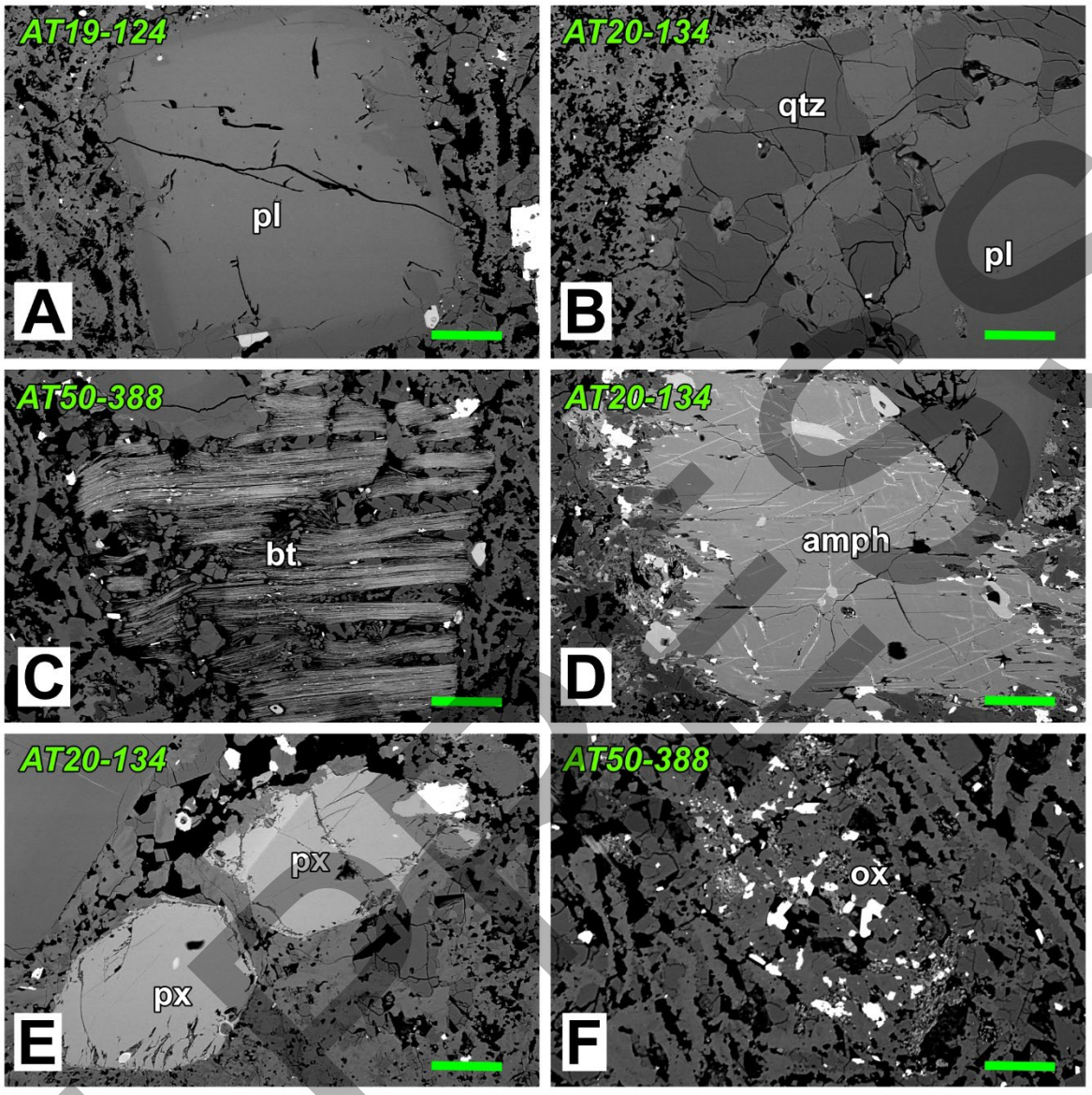

Fig. 4. Backscattered electron images (BSE) of samples from the Patao Ignimbrite. **A.** Euhedral plagioclase phenocryst developing concentrical normal zoning. **B.** Crystal clot of anhedral quartz and subhedral plagioclase. **C.** Subhedral biotite phenocryst. **D.** Subhedral amphibole crystal with dehydration rim. **E.** Pair of euhedral pyroxene phenocrysts. **F.** Oxide-rich lithic clast. The green line is 100 μm long. The matrix in all the images is composed of microphenocrysts of quartz, plagioclase and glass shards.

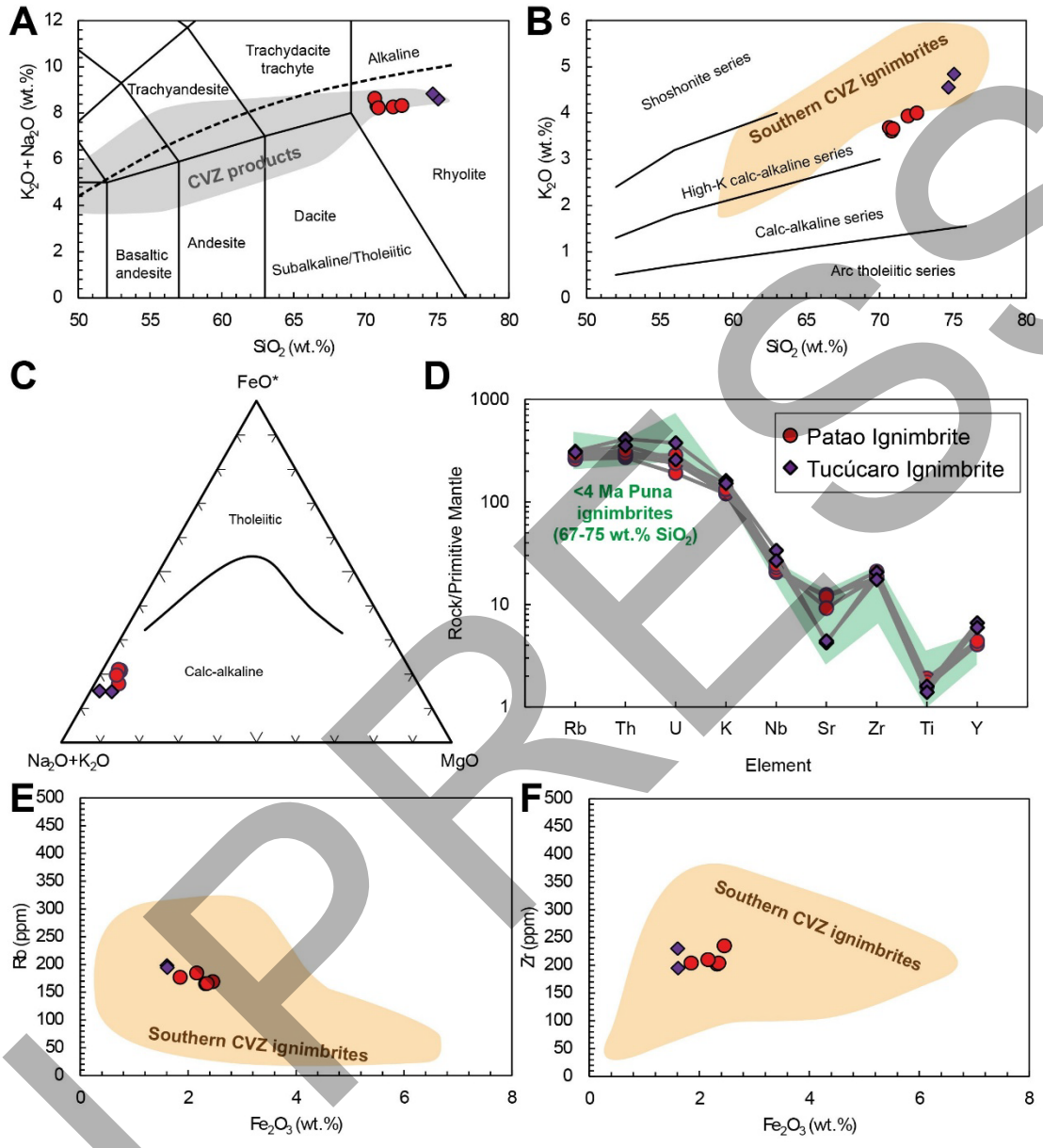

Fig. 5. A. Geochemistry of the Tucúcaro (Ureta et al., 2020) and Patao (this work) ignimbrites. The grey field of the CVZ products is taken from Mamani et al. (2010). **B.** K_2O vs. SiO_2 diagram. Clear brown field of southern CVZ ignimbrites after Schnurr et al. (2007). **C.** AFM diagram. Boundary between the calc-alkaline and tholeiitic fields after Irvine and Baragar (1971). **D.** Spider diagram of selected trace elements normalised to primitive mantle (Sun and McDonough, 1989). The green field is based on the data of Kay et al. (2010). **E-F.** Rb and Zr vs. Fe_2O_3 plots, respectively, for southern CVZ ignimbrites (clear brown field) after Schnurr et al. (2007). The kinked trends for Zr and Ba suggest a two-stage fractionation.

Table 1. Whole-rock major and trace element geochemistry of the Patao ignimbrite samples studied in this work. The location of the sampling sites is given in figure 1.

Sample	AT19-124	AT20-134	AT26-180	AT50-388	AT50-394
SiO_2 (wt.%)	70.11	69.95	70.07	70.97	71.70
TiO_2	0.38	0.41	0.41	0.34	0.37
Al_2O_3	15.09	14.82	15.19	13.71	14.05
Fe_2O_3	2.30	2.43	2.33	1.83	2.14
MnO	0.08	0.09	0.10	0.06	0.08
MgO	0.51	0.53	0.44	0.65	0.46
CaO	2.20	2.13	2.03	2.85	1.70
Na_2O	4.64	4.89	4.51	4.26	4.27
K_2O	3.57	3.65	3.62	3.88	3.96
P_2O_5	0.09	0.10	0.13	0.10	0.12
Total	99.00	99.00	98.82	98.66	98.85
Nb (ppm)	14.6	16.2	15	16.3	17.4
Zr	202	235	204	204	210
Y	18.4	19.5	20	18.5	19.9
Sr	262	250	250	195	193
U	4	5	5	6	5
Rb	165	169	165.6	176.6	184.4
Th	23	24	25	25	27
Pb	10	11	14	11	12
Ga	16	16	16	15	16
Zn	35	39	39	27	36
Ni	3	2	4	3	3
Cr	11	1	3	3	0
V	13	18	15	14	15

Table 2. Summary of observations and their corresponding interpretative criteria regarding the evidence supporting the existence of the Tálar Caldera.

Evidence	Characteristics	Interpretation
Geomorphology	29×20 km oval shaped depression, surrounded by a topographic rim and scarps up to 700 m high built on Miocene volcanics. It hosts the Tálar and Capur salt flats.	Sub-circular, piston-like caldera covering an area of 310 km^2 and an approximate depression volume of 114 km^3.
Stratigraphy	Two superimposed ignimbrite units with similar extent and componentry (TI and PI), both with an age of ~2.5 Ma. Maximum unit thicknesses observed near the rim or within the depression (55-125 m). Distal facies are 10-30 m thick.	Ignimbrites preserved as both intracaldera and outflow facies, mainly distributed toward the W and NW. In total, they represent ~53 km^3 (~40 km^3 DRE) of preserved deposits.
Geochemistry and petrology	Compositionally and geochemically similar rhyolitic products (TI and PI).	Two phases of the same volcanic event or two successive eruptions shortly spaced in time.
Geomorphology	10×6 km oval bulge nearly at the centre of the depression, up to 200 m high above its floor. It has a well-developed extensional suite of NE-trending faults and a volcano on top (Caichinque).	Resurgent dome approximately at the geometrical centre of the caldera, with an apical graben and a post-collapse stratocone.

Table 3. Age, caldera area, and ignimbrite bulk volume for flare-up events younger than 9 Ma in the Central Volcanic Zone of the Andes, with stress in the Altiplano-Puna Volcanic Complex.

Caldera			Ignimbrite(s)			
Name	**Area (km^2)**	**Type**	**Name**	**Age (Ma)**	**Volume (km^3)**	**Ref.**
Cerro Blanco	45	Piecemeal	Cerro Blanco	0.0042	15.2	4
Cerro Blanco	-	Volcano-tectonic	Campo de Piedra Pómez	0.007	15.5	4
Incapillo	-	Piston	Incapillo	0.51	20.4	5
Tatio	12	-	Tatio	0.7	53	3
Purico Complex	19	-	Purico	1.3	100	2
Cerro Galán	810	-	Cerro Galán	2.3	630	5
Tálar	310	Piston	Patao	2.5	23	7
Pastos Grandes	1300	-	Pastos Grandes	2.89	2000	3
Tálar	310	Piston	Tucúcaro	3	30	7
Cerro Guacha	170	-	Tara	3.49	1066	3
Laguna Escondida	580	Piston	Laguna Verde	4	500	6
La Pacana	1155	Trapdoor	Atana	4	2500	1

Wheelwright	271	Piston	Wheelwright	5	80	6
Alto Parinas	63	Piston	Las Parinas	5	10	6
Cerro Guacha	1300	-	Cerro Guacha	5.65	1733	3
Coranzulí	171	Boiling over	Corral de Sangre/Las Termas/Potreros/Abra Grande	6.6	650	5
Panizos	346	Trapdoor/downsag	Cerro Panizos	6.8	652	3
Yerbas Buenas	-	-	Sifón	8.33	2400	3
Vilama	490	Trapdoor / Piston	Vilama	8.4	1200	5

[1] Lindsay et al. (2001), [2] Schmitt et al. (2001), [3] Salisbury et al. (2011), [4] Báez et al. (2015), [5] Guzmán et al. (2017), [6] Naranjo et al. (2018), and [7] this work.

The location of many of these calderas is available on figure 1.